Polymer 50 (2009) 5518–5532

Contents lists available at ScienceDirect

Polymer

journal homepage: www.elsevier.com/locate/polymer

Reactivity, viscoelastic behaviour and mechanical performances of hybrid systems based on epoxy resins and reactive polyhedral oligosilsesquioxanes☆

Giuseppe Ragosta*, Pellegrino Musto, Mario Abbate, Gennaro Scarinzi

Institute of Chemistry and Technology of Polymers, National Research Council of Italy, via Campi Flegrei, 34, Olivetti Building, Pozzuoli (NA) 80078, Italy

ARTICLE INFO

Article history:
Received 10 July 2009
Received in revised form
11 September 2009
Accepted 18 September 2009
Available online 22 September 2009

Keywords:
Epoxy resins
Mechanical properties
NIR spectroscopy

ABSTRACT

An epoxy formulation was modified by adding various amounts of an epoxy functionalized polyhedral oligomeric silsesquioxane (POSS). The obtained networks were characterized in terms of reactivity, viscoelastic behaviour and mechanical properties. Spectroscopy measurements by FT-NIR demonstrated that the epoxy groups of POSS were almost as reactive as those of the DGEBA in the curing stage, while in the post-curing a lower reactivity of the latter was found, possibly due to steric hindrance effects. The dynamic-mechanical analysis showed an increase in the storage modulus in both glassy and rubbery regions. On the other hand, T_g and T_β decreased with POSS content. The viscoelastic analysis showed that the addition of POSS enhanced the free volume and the tendency of the network to undergo thermal expansion. In particular, the β transition was made increasingly localized by increasing the POSS content. With respect to mechanical performances, the yield process was facilitated by incorporation of the POSS nanocages within the network, possibly due to an enhancement of the chain mobility. Fracture measurements showed an improvement of the parameters K_c and G_c up to 5 wt% of POSS, after which a decrease of toughness was observed. These results were supported by a fractographic analysis.

1. Introduction

A variety of particulate fillers are used in thermosetting resins, primarily to reduce thermal shrinkage in the manufacture of castings or moulded products and to lower the coefficient of thermal expansion of finished products [1,2]. For coating applications fillers are used to increase the hardness and the abrasion resistance [3].

Particulate fillers used in polymers normally have particle size in the range of 5–100 μm in diameter and are used at around 15–30 v%. The maximum amount used is limited by the resulting deterioration in processing characteristics and fracture toughness. In particular, the fracture toughness is also dependent on the nature of the filler. For instance Brown et al. [4] and Azimi et al. [5] have demonstrated significant increases in the fracture toughness of DGEBA epoxies that can be achieved through the inclusion of fluid filled or hollow microcapsules and rigid microspheres. As the filler size decreases to smaller than 100 nm, the resulting composites, termed nanocomposites, may show dramatic improvements in such properties as gas barrier, thermal-oxidative and photo-oxidative stability, elastic modulus and mechanical and fracture properties. When these effects occur, they can be generally achieved at relatively lower filler content in comparison to conventional microcomposites, due to the extremely high surface to volume ratio which, in turn, emphasizes the interfacial interactions and the filler surface properties [6,7]. The physical properties of polymeric nanocomposites are primarily determined by their morphological features, i.e. the homogeneity and degree of dispersion of the inorganic phase within the polymer matrix. It is well known that the surface energy dramatically increases by decreasing the particle size, so that the nanofillers invariably tend to aggregate. The achievement of a homogeneous nanoscale dispersion of the filler, with no or reduced aggregation represents a major challenge in this area.

The polyhedral oligomeric silsesquioxanes (POSS) are an important class of organic–inorganic compounds which have been successfully employed as precursors of nanocomposites [8–10]. In particular, the compounds of general formula $R_8Si_8O_{12}$ are well defined, highly symmetrical molecules with a cubic inorganic core (the cage) with T_8 structure, surrounded by eight equivalent organic moieties (R) covalently bound to the silicon atoms. Here the term T refers to silicon NMR nomenclature and indicates silicon atoms bound to three oxygen atoms. A single POSS molecule has a diameter of approximately 1.5 nm, including the organic groups. These form a voluminous shell around the Si_8O_{12} cage, comprising about 80% of the total volume, and effectively control the interactions

☆ Presented in part at the Conference "Frontiers in Polymer Science", Mainz, Germany, 7–9 June, 2009.

* Corresponding author.
E-mail address: rago@ictp.cnr.it (G. Ragosta).

0032-3861/$ – see front matter © 2009 Elsevier Ltd. All rights reserved.
doi:10.1016/j.polymer.2009.09.049

between the POSS units and the surrounding matrix. It is possible to tailor-make the organic shell so as to render the POSS units compatible with numerous polymers and biopolymers; furthermore, functional groups can be introduced to allow the possibility of incorporating POSS into polymer chains or networks by covalent bonding [8]. In particular, several literature studies have reported on the preparation and characterization of epoxy/POSS nanocomposites where the functionalities of the modifier were either primary amines or epoxy groups. Interesting results were achieved in terms of increment of thermomechanical properties, lowering of dielectric constant and, above all, increase of thermal and oxidative stability [11–14]. Several authors [15–18] reported a molecular level reinforcement although the mechanism responsible for this effect is still uncertain. According to Lee et al. [16] the reinforcement provided by the POSS cages retards the physical aging of the epoxy resin in the glass state. A strong effect of the *R* groups type was found by other investigators on the dynamic-mechanical response, fracture toughness and thermal stability [17–20]. Equally important was found the morphology of the hybrid systems and the degree of phase separation of the POSS phase, which was tuned adjusting the degree of reaction between the epoxy matrix and the POSS component [12,21–23]. In the present study an epoxy network structure made of diglycidyl ether of bisphenol-A (DGEBA) and diamino diphenylsulfone (DDS) was modified by incorporation of varying amounts of epoxy terminated POSS. In the first part of this work the reactivity of the system components were investigated by means of Fourier Transform Near Infrared Spectroscopy (FT-NIR). The aim was to study the network formation process and the molecular structure obtained therefrom, with particular emphasis given to the influence of the POSS reactive groups on the mechanism and kinetics of the curing and post-curing stages. The second part is focused on the analysis of the dynamic-mechanical behaviour of the modified epoxy resins in comparison to that of the parent network, in an attempt to rationalize the complex effects of the nanofiller on the viscoelastic properties of the materials. The use of a technique capable of probing segmental motions as well as larger scale transitions allowed us to gather information on the complex molecular structure of the networks and on the influence of the POSS nanocages on the free volume and molecular mobility of the systems. Finally, the yielding and fracture properties were measured and interpreted in the light of the molecular structure and on the basis of a fractographic analysis of the samples' surfaces.

2. Experimental

2.1. Materials

Diglycidyl ether of bisphenol-A (DGEBA), diamino diphenylsulfone (DDS) and OctaGlycidyldimethylsilyl-POSS (OG-POSS) were purchased from Sigma–Aldrich Italy. These products were used as received, with no further purification. Toluene was a Lab-Scan analytical grade solvent, also from Aldrich.

The chemical formulas of the mixture components are reported below:

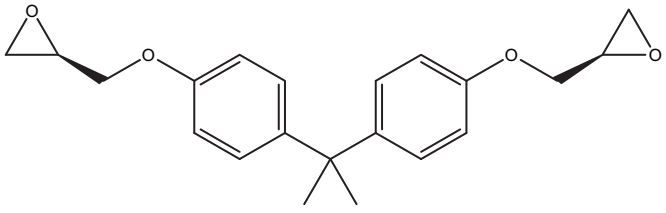

DGEBA

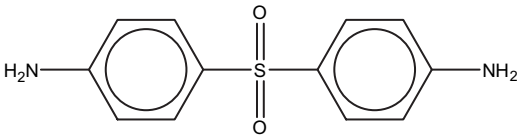

DDS

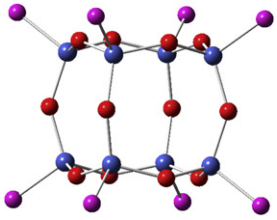

OG-POSS

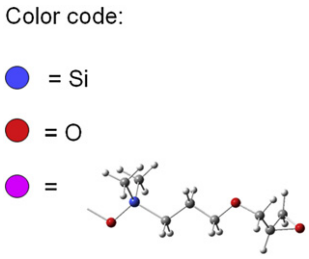

2.2. Preparation of a typical epoxy/DDS/OG-POSS nanocomposites

6.76 g of DGEBA, 2.40 g of OG-POSS and 6.0 mL of toluene were placed in a round-bottomed glass flask. The mixture was stirred at 40 °C for 30 min, thereafter applying vacuum to remove toluene. Upon complete solvent elimination, the temperature was raised to 140 °C and 2.84 g of DDS were added. This formulation corresponds to a final composition of the nanocomposite DGDDM/DDS/OG-POSS 56/24/20 wt%. The mixture was mechanically stirred up to complete dissolution of the diamine hardener, degassed under vacuum and cast in a glass mould treated by a releasing agent (Lubrolene E&, kindly supplied by Finco Srl, Italy). Curing was carried out at 140 °C for 16 h, and post-curing at 180 °C for 4 h. With the above protocol several formulations were prepared, as detailed in Table 1.

Table 1
Composition of the prepared mixtures.

Code	DGEBA (wt%)	DDS (wt%)	POSS-OG (wt%)	DGEBA[a] (mol%)	DDS[b] (mol%)	POSS-OG[a] (mol%)	*R*[c]
N0	75.2	24.8	–	50.0	50.0	–	–
N5	70.5	24.5	5.0	47.4	50.0	2.6	18.2
N10	65.8	24.2	10.0	44.7	50.0	5.3	8.4
N20	56.3	23.7	20.0	39.1	50.1	10.8	3.6

The ratio [epoxy]/[NH] is always = 1.
[a] Moles of epoxy groups over the total amount of reactive groups.
[b] Moles of N–H groups over the total amount of reactive groups.
[c] $R = [\text{epoxy}]_{\text{DGEBA}}/[\text{epoxy}]_{\text{POSS-OG}}$.

2.3. Techniques

FT-NIR spectra were collected with a System-2000 spectrometer from Perkin–Elmer. This instrument was equipped with a high temperature tungsten halogen NIR source, a quartz beam-splitter and a deuterated triglycine sulphate (DTGS) detector. The measurements were performed in the transmission mode on 1.30 mm thick samples in the wavenumber range 8000–4000 cm^{-1} at a resolution of 4 cm^{-1}. A minimum of 32 scans were co-added for each measurement to improve the signal-to-noise ratio. The isothermal kinetic measurements were carried out in a Specac 20100 temperature chamber modified in-house, which was fitted in the sample compartment of the spectrometer for the in-situ collection of spectral data. The curing process was carried out at 140 °C for 13 h, followed by post-curing at 180 °C for 4 h. Both processes were carried out under a continuous flux of dry N_2 (60 $cm^3\,min^{-1}$).

Dynamic-mechanical tests were carried out on samples with dimensions 50 × 10 × 1.0 mm using a Perkin–Elmer Pyris Diamond DMA apparatus. Tests were performed in bending mode, applying a strain of 1%. Single-frequency measurements at 1 Hz were performed at constant heating rate of 3 °C/min, in the temperature range from −150 °C up to 300 °C. Multi-frequency tests were performed at constant heating rate of 0.5 °C/min in the temperature range from −150 °C up to 250 °C and at the frequencies of 0.05, 0.1, 0.2, 0.5, 1, 2, 5, 10 and 20 Hz.

Mechanical tests were performed using a universal testing machine, Instron model 4505. Values for the flexural modulus were obtained from the tangent of the force/deflection curve using 3-point bending tests (ASTM D790 method) with rectangular specimens, 60.0 × 6.0 × 4.0 mm, and a span/width ratio of 8:1. The measurements were carried out at a cross-head speed of 1 mm/min, and at ambient temperature.

The yield strength was measured in compression on specimens, 60.0 × 6.0 × 4.0 mm, loaded along the length. The tests were carried out at different cross-head speeds and temperatures. At least four samples for each cross-head speed and temperature were used. Due to the absence of a definite maximum in the load/deformation curves the yield strength was estimated as the stress corresponding to the 5% offset strain from the elastic strain.

Fracture toughness was assessed using a multiple crack length procedure on V-notched rectangular specimens, 60.0 × 6.0 × 4.0 mm, SEN types with notch length varying from, 1.5 to 4.5 mm, extended by 0.2 mm by a razor blade fixed to a micrometer apparatus. At least three samples for each notch length were used. The final length of the notch was measured using an optical microscope after fracturing the specimens. The tests were conduced at a cross-head speed of 1 mm/min and at ambient temperature.

The critical stress intensity factor, K_c, was calculated according to the following equation:

$$K_c = Y\sigma\sqrt{a} \tag{1}$$

where σ is the stress calculated as the outer skin stress for a rectangular beam in 3-point bending, Y is the compliance calibration factor obtained from tables quoted in the literature [24] and a is the notch length.

The critical strain energy release rate, G_c, was estimated through the equation:

$$G_c = \frac{U}{BW\phi} \tag{2}$$

where U is the energy at fracture initiation, B and W are the thickness and the width of the specimen, respectively, and ϕ is a correction factor that takes into account the rate of change of compliance, C, with crack length:

$$\phi = C\left[\frac{dC}{d\left(\frac{a}{W}\right)}\right]^{-1} \tag{3}$$

The values of ϕ were obtained from the tables reported in the literature [25].

The morphology of the samples was examined on fractured samples by scanning electron microscopy (SEM). The apparatus used was a Philips SEM mod. XL20 and the fracture surfaces were coated with a thin layer of gold–palladium of about 5 nm by vacuum sputtering.

3. Results and discussion

3.1. Analysis of the curing process by NIR spectroscopy

In Fig. 1 are represented the NIR spectra in the wavenumber range 8000–4000 cm^{-1}, of the DGEBA monomer and of OG-POSS. The DGEBA spectrum displays two intense absorptions originating from the epoxy functionality, located at 6065 and at 4532 cm^{-1}. These were attributed, respectively, to the first overtone of the terminal CH_2 stretching mode (2 × 3054 cm^{-1}) and to a combination band between the epoxy CH_2 stretching and the epoxy CH_2 deformation (3054 + 1456 cm^{-1}) [26–28]. Partially resolved peaks at 5987, 5917 and 5887 cm^{-1} were assigned, respectively to the overtone of the phenyl ν(C–H) (2 × 3020 cm^{-1}), the overtone of the epoxy $\nu_s(CH_2)$ (2 × 2997 cm^{-1}) and a combination of the epoxy $\nu_s(CH_2)$ and ν(C–H) modes (2997 + 2930 cm^{-1}) [24,26]. A peak due to the combination of the aromatic ν(CH) and the aromatic ν(C=C) fundamentals (3040 + 1607 cm^{-1}) is detected at 4680 cm^{-1}, while at 4622 cm^{-1} is found a related combination involving another aromatic ν(C=C) at lower frequency (3040 + 1509 cm^{-1}). Finally, at 4065 cm^{-1} is found a further aromatic combination involving the aromatic ν(CH) and the ν_s(Ph–O–C) fundamental (3040 + 1034 cm^{-1}) [28].

The NIR spectrum of OG-POSS (reported for the first time, to our knowledge) displays the two intense epoxy signals at about the same positions previously found for the DGEBA monomer

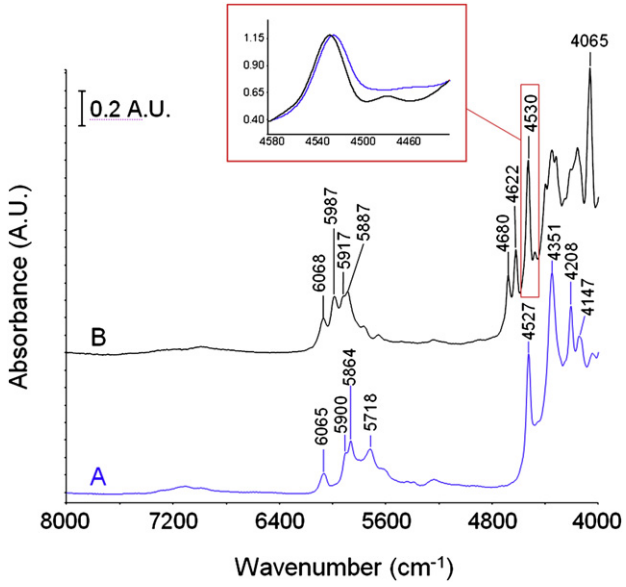

Fig. 1. FT-NIR spectra in the wavenumber range 8000–4000 cm^{-1} of: (A) liquid OG-POSS; (B) DGEBA monomer. The inset highlights the frequency difference of the respective epoxy peaks.

(respectively, at 6065 and 4527 cm^{-1}). Both peaks, however, are slightly displaced towards lower wavenumbers, and the 4527 cm^{-1} peak could be, under favourable circumstances, spectroscopically resolved (see the inset of Fig. 1).

In order to investigate the reactivity of the formulation components, and, in particular, that of the OG-POSS additive, we performed in-situ isothermal kinetic measurements by *time-resolved* NIR spectroscopy. The kinetic analysis was carried out at 140 °C (T_{cure}) and, subsequently, on the same sample, at 180 °C ($T_{post\text{-}cure}$). Among the different compositions prepared, the one containing 20 wt% of OG-POSS was chosen for the analysis since, for lower OG-POSS contents, no detectable differences were found in the curing kinetics with respect to the plain epoxy resin.

In Fig. 2 are reported the FT-NIR spectra of the uncured DGEBA/DDS/OG-POSS admixture (trace A), and the spectra of the same admixture after curing at 140 °C (trace B) and post-curing at 180 °C (trace C). The above spectra closely resemble those collected in the same conditions on a control resin made of DGEBA/DDS only, and already reported in previous literature studies [29]. This because the inorganic part of OG-POSS contributes very little to the NIR spectrum, while the organic part provides signals that are very close to and thus barely distinguishable from those of the DGEBA.

The evolution of the NIR spectrum of the DGEBA/DDS/OG-POSS admixture is represented in Fig. 3 in the more significant wavenumber ranges. In Fig. 3a is reported the 7540–6200 cm^{-1} interval, where the initial spectrum shows a two component band at 7005–6905 cm^{-1} arising from the first overtone of the ν(OH) modes (compare also the inset of Fig. 2). The shape of this band reflects a complex (bimodal) distribution of hydrogen-bonding aggregates in the uncured system. The band is found to increase gradually as the curing proceeds, owing to the production of hydroxyl groups by the epoxy/amine addition. The bandshape evolves becoming more symmetrical and the initial two component structure is gradually lost. It appears that a more homogeneous H-bonding network in terms of donor–acceptor pairs is realized at the end of the curing process with respect to that initially present. This is partly due the presence, in the uncured admixture, of H-bonding groups (primary amines) which compete with the hydroxyls; these are completely depleted on curing. Owing to its symmetry, intensity and resolution, the area of the OH band appears to be well suited for quantitative analysis.

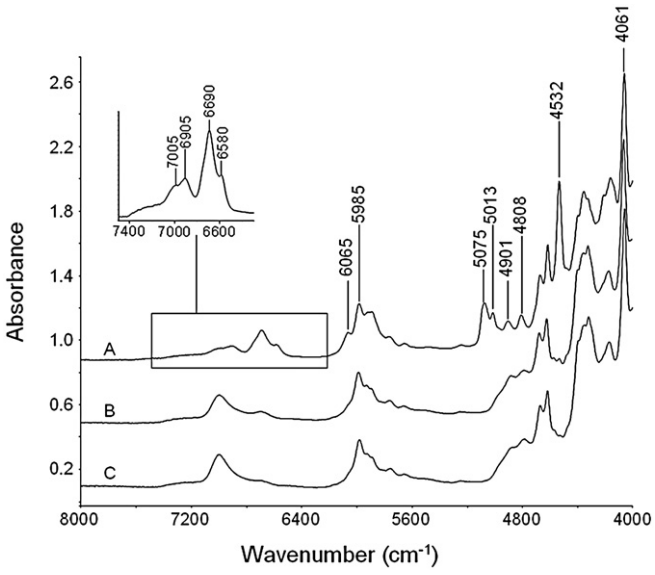

Fig. 2. FT-NIR spectra of: (A) uncured DGEBA/DDS/OG-POSS mixture with 20 wt% of OG-POSS; (B) mixture cured at 140 °C for 12 h; mixture post-cured at 180 °C for 3 h. The inset evidences the ν(O–H), ν(N–H) region for the spectrum of the uncured mixture.

Fig. 3b displays the 6390–5500 cm^{-1} wavenumber range. A gradual reduction of intensity is observed at 6065 cm^{-1} (epoxy peak) and at 5920 and 5890 cm^{-1}. On the other hand, the decrease of the peak at 5985 cm^{-1} seems to be related to the decrease of its neighbouring, partially overlapped peaks. These observations can be rationalized in view of the previously discussed assignments. Severe peak overlapping prevents their use for analytical purposes.

In Fig. 3c is depicted the 5400–4700 cm^{-1} interval whose main features are represented by the doublet at 5075–5013 cm^{-1} due, respectively, to the combination modes $\nu_{as}(NH_2)+\delta(NH_2)$ (3460 + 1630 cm^{-1}) and $\nu_s(NH_2)+\delta(NH_2)$ (3370 + 1630 cm^{-1}) [26–28]. Owing to its considerable intensity and limited interference from neighbouring bands, this doublet provides a precise measure of the primary amine concentration in the system. It is noted that the doublet goes to zero, thus indicating the complete consumption of primary amine groups after the curing cycle. A broad band in the range 5000–4750 cm^{-1} is found to increase as curing proceeds and is assigned to a combination of the O–H stretching and bending fundamentals ($\approx$3550 cm^{-1} + $\approx$1450 cm^{-1}). Finally, in Fig. 2D is shown the 4840–4100 cm^{-1} interval with the analytical epoxy peak at 4532 cm^{-1}, discussed earlier.

Sequences of spectra as those represented in Fig. 3 provide a mean to quantify the concentration of the reacting groups as a function of time. In particular, the relative conversion of epoxy and primary amine groups can be evaluated in the usual way as:

$$\alpha = \frac{C_0 - C_t}{C_0} = 1 - \frac{C_0}{C_t} = 1 - \frac{A_t}{A_0} \tag{4}$$

where A is the absorbance value at 4532 cm^{-1} for the epoxy groups and at 5075 cm^{-1} for the primary amine. The subscripts 0 and t denote reaction times.

In Fig. 4 are reported the curves epoxy conversion versus time relative to the control resin and to the formulation containing 20% wt/wt of OG-POSS. Both curves display an initial pseudo-linear regime, followed by a plateau region which is reached after about 400 min. In order to describe the complex reaction kinetics of epoxy/amine systems, several models have been put forward, mostly based on simplifying assumptions made on a set of elementary reaction steps describing the epoxy/amine polymerization mechanism (semi-empirical models). The more popular kinetic equations are those of Horie [30]:

$$\frac{d\alpha}{dt} = (k_1 + k_2\alpha)(1-\alpha)^2 \tag{5}$$

and Kamal [31,32]:

$$\frac{d\alpha}{dt} = (k_1 + k_2\alpha^m)(1-\alpha)^n \tag{6}$$

In both equations the Arrhenius-type rate-constants k_1 and k_2 account for the autocatalytic nature of the mechanism, with the former being related to the catalysis of the groups initially present in the resin and the latter corresponding to the catalytic activity of hydroxyl groups formed by the epoxy/amine addition. It is noted that the Horie equation assumes equal reactivity of primary and secondary amino-hydrogens, which is verified for aliphatic but not for aromatic amines. Thus, the Horie model is inappropriate in the present case.

Recently, Cole [33] developed a more rigorous kinetic model and concluded that the process could be divided into two stages, the first being dominated by the epoxy/amine addition and reasonably well described by eq. (5) or (6). At the later stages of cure, however,

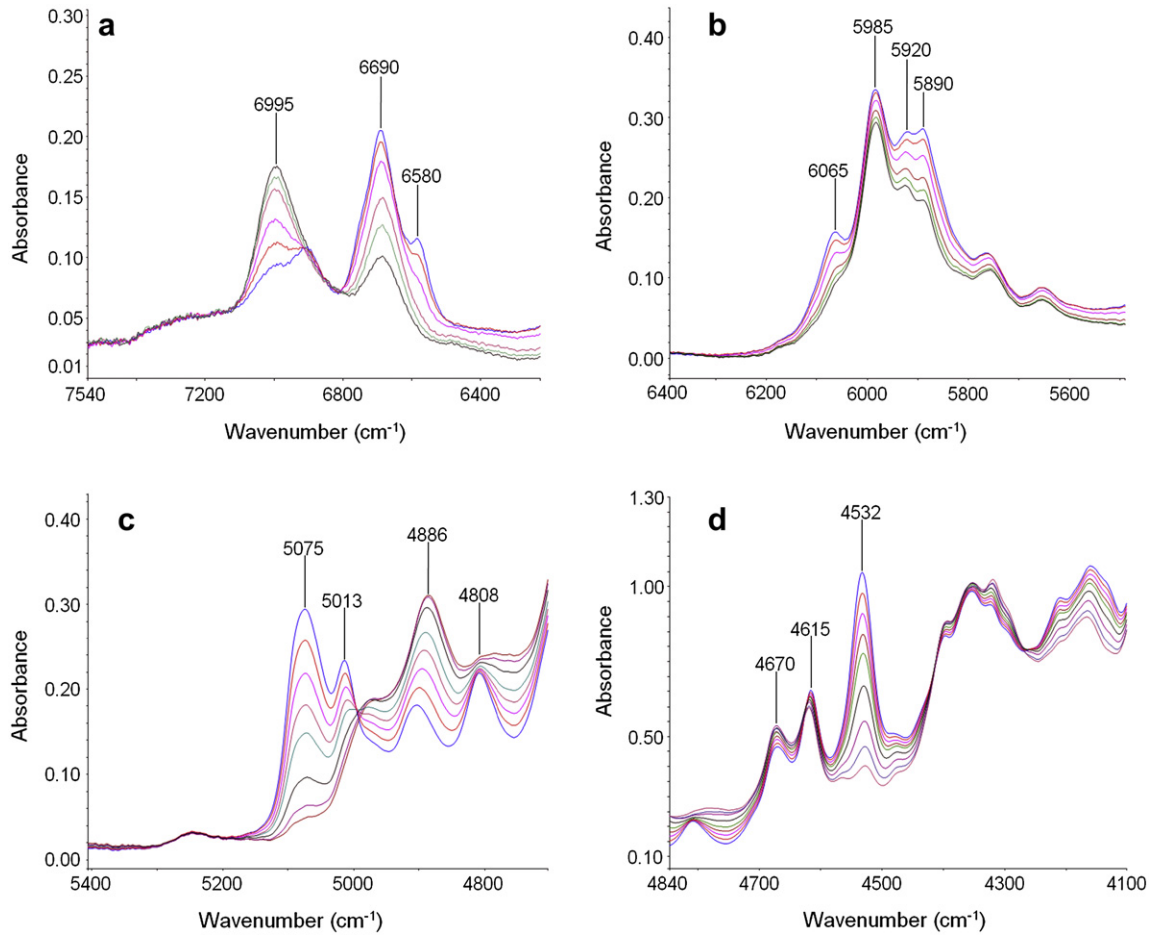

Fig. 3. *Time-resolved* FT-NIR spectroscopy for monitoring the isothermal curing kinetics of the DGEBA/DDS/OG-POSS mixture (composition 56/24/20 wt%).

the isothermal cross-linking reaction approaches a simple first-order regime with respect to epoxide concentration; the relevance of this regime with respect to the previous one depends on cure temperature and on the reactivity of the components. In the present case it is found that a first-order homogeneous model of the form:

$$\frac{d\alpha}{dt} = k(\alpha_{max} - \alpha) \tag{7}$$

which, upon integration yields:

$$\alpha = \alpha_{max}\left(1 - e^{-kt}\right) \tag{8}$$

is able to satisfactory fit the experimental data in the whole conversion range for both the plain DGEBA/DDS resin and the OG-POSS containing formulation (correlation coefficients, R^2, equal to 0.996 and 0.995, respectively). More complex model equations, such as eq. (6), were found not to improve the situation. In this context, introducing α_{max} in place of 1 in eq. (7) is meant to account for the incomplete epoxy conversion in the plateau region, caused by the system T_g approaching the reaction temperature [34]. The reason why the first autocatalytic regime is not apparent in the present kinetic data is to be related, in our opinion, to the relatively high cure temperature (140 °C) which speeds up the process thereby reducing the impact of the catalytic activity on the overall mechanism. The kinetic analysis evidences that the rate-constant for the control resin is almost coincident with that of the OG-POSS containing formulation ($k = 0.0131$ and 0.0119 min^{-1}, respectively), while the plateau conversion is nearly complete for the former resin (0.97) and only slightly lower for the latter (0.95). Recalling that, for the resin modified by OG-POSS, α represents an overall epoxy conversion, i.e. it comprises oxirane rings from both the DGEBA and the OG-POSS components, the

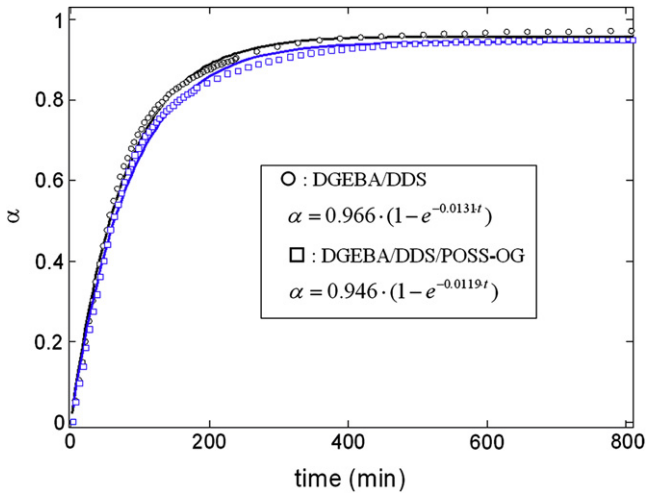

Fig. 4. Relative conversion (α) of epoxy groups as a function of time for the isothermal curing at 140 °C. Symbols refer to the data points (as indicated in the legend), lines are relative to the 1st order fit.

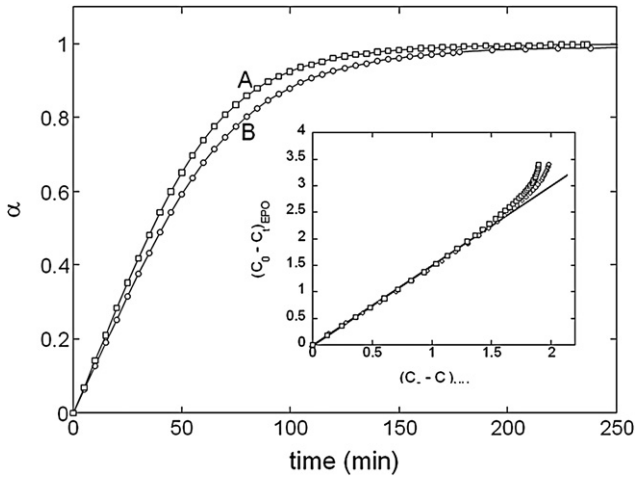

Fig. 5. Relative conversion of primary amine groups as a function of time for the isothermal curing at 140 °C. (□): mixture composition DGEBA/DDS 75/25 wt%; (○): mixture composition DGEBA/DDS/OG-POSS 56/24/20 wt%. Curves are for eye guidance only.

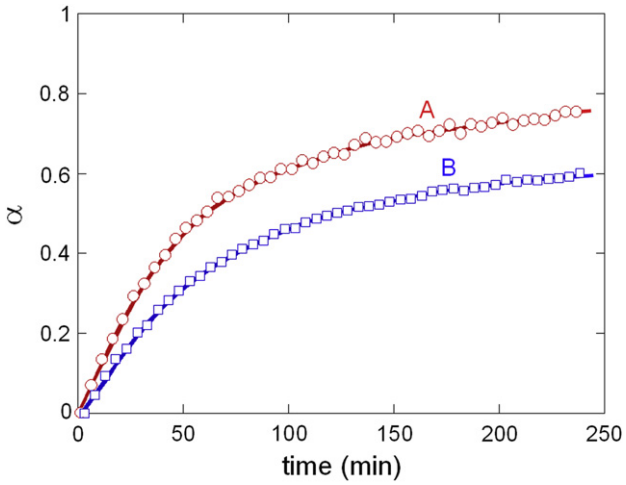

Fig. 7. Relative conversion (α) of epoxy groups as a function of time for the post-curing at 180 °C. (A): mixture composition DGEBA/DDS 75/25 wt%; (B): mixture composition DGEBA/DDS/OG-POSS 56/24/20 wt%. Curves are for eye guidance only.

above results point to a reactivity of the OG-POSS functionalities almost coincident to that of the DGEBA, at least in the present curing conditions.

Fig. 5 depicts the relative conversion of primary amine groups in the control resin (curve A) and in the OG-POSS containing resin (curve B). In both cases the consumption of primary amine is complete after about 200 min, and a slightly lower reaction rate for the modified epoxy formulation is again observed. By plotting the kinetic data on an epoxy – primary amine conversion–conversion diagram [absolute conversions need to be used for this analysis, i.e. $C_0 - C_t = (1 - (A_t/A_0)) \cdot C_0$], it is possible to derive information about the stoichiometry of the process, the reactivity of the components and to detect possible changes of mechanism with conversion [29,35]. A plot of this type relative to the plain epoxy resin and to the resin modified by OG-POSS, is represented in the inset of Fig. 5. Both data sets can be accommodated on a single straight line encompassing most of the range of primary amine conversion. In fact, the curve upturn starts at $C_0 - C_t$ values of 1.7 mol/kg (with the OG-POSS containing system deviating slightly before than the control), which correspond to 85% primary amine conversion. The slope of the straight line is 1.5, i.e. the ratio between reacted epoxy groups and primary amines end is 3:2. Assuming that, in the steady regime etherification plays a negligible role in the overall mechanism, this means that three epoxy groups react with two primary and one secondary amine. This mechanism and stoichiometry hold constant up to the almost complete depletion of the primary amine, after which etherification is likely to contribute more substantially. The presence of a considerable amount of epoxy groups linked to the OG-POSS cages is found not to alter significantly the mechanism of the curing process, thus confirming an almost equivalent reactivity in comparison to the DGEBA oxirane rings.

In Fig. 6 are compared the concentration profiles of the hydroxyl groups formed on curing, expressed in terms of the normalized absorbance of the O–H band at 6995 cm^{-1} (i.e. $\bar{A}_{6995} = A_{6995}/A_{4065}$) for the unmodified (curve A) and the OG-POSS modified (curve B) resins. In the initial linear regime the two curves are coincident, while the latter prevails significantly at the later stages of cure. The two concentration profiles start to deviate from each other at about

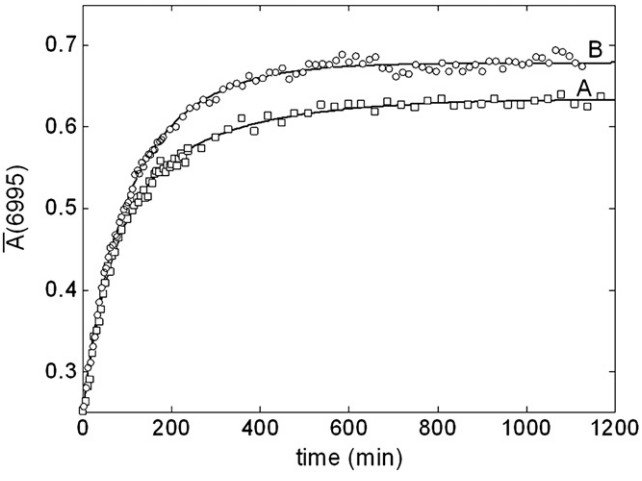

Fig. 6. Normalized absorbance of the OH band at 6995 cm^{-1} as a function of time for the isothermal curing at 140 °C. (□): mixture composition DGEBA/DDS 75/25 wt%; (○): mixture composition DGEBA/DDS/OG-POSS 56/24/20 wt%. Curves are for eye guidance only.

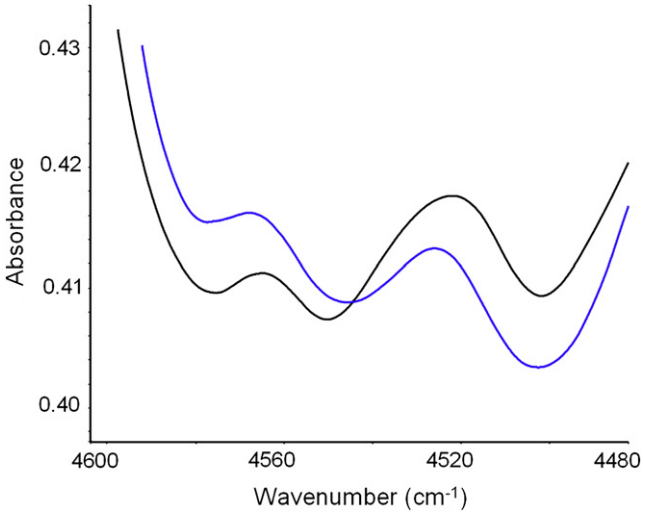

Fig. 8. Comparison between the epoxy peaks at the beginning of the post-curing process. Trace A: mixture composition DGEBA/DDS 75/25 wt%; Trace B: mixture composition DGEBA/DDS/OG-POSS 56/24/20 wt%.

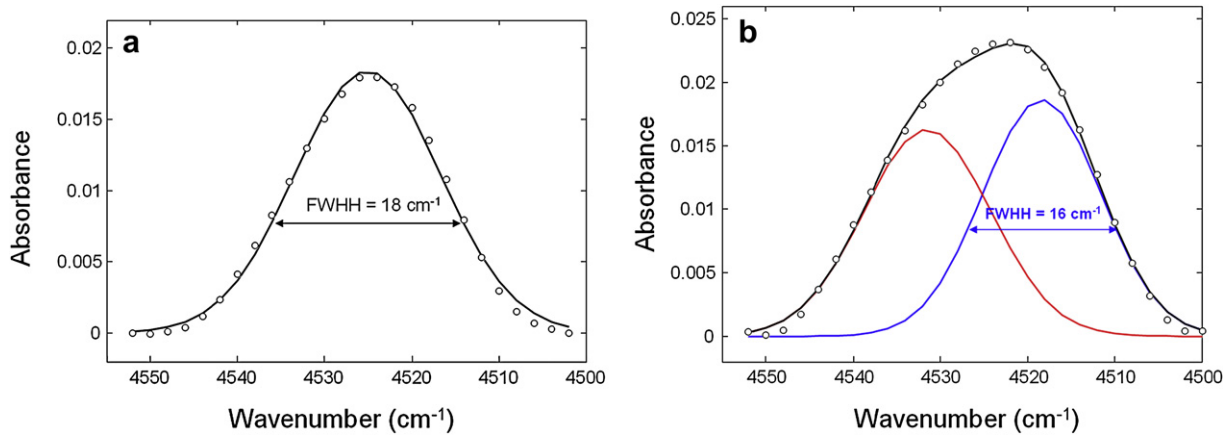

Fig. 9. Curve-fitting analysis of the epoxy peak at 1432 cm^{-1}. (a): mixture composition DGEBA/DDS 75/25 wt%; (b): mixture composition DGEBA/DDS/OG-POSS 56/24/20 wt%. Open circles = experimental data points; black trace = simulated profile; blue and red traces = band components. (For interpretation of the references to colour in this figure legend, the reader is referred to the web version of this article.)

200 min, i.e. after the almost complete depletion of primary amine. Thus, in the presence of primary amine the reaction mechanism is the same, but afterwards the OG-POSS containing system produces more hydroxyls, i.e. more epoxy-secondary amine addition than the neat resin, for which the etherification is more relevant. In fact etherification occurs with consumption of epoxy groups and no net production of O–H groups.

3.2. Post-curing

The post-curing of the two investigated formulations brings about detectable changes in the respective NIR spectra. In particular, the epoxy signals at 4532 cm^{-1} and the secondary amine band at 6680 cm^{-1} decrease further (compare Fig. 2B and C). In Fig. 7 the relative conversion of epoxy groups (relative to those initially present at the beginning of the post-curing) is reported as a function of time for the two investigated formulations. The diagram evidences that, despite a higher initial concentration of reactants, the modified resin shows a significantly lower reactivity (i.e. slower rate and lower conversion values) in comparison to the control resin, contrary to what is found in the curing stage.

A closer inspection of the epoxy band of the two formulations (Fig. 8) evidences some differences: contrary to the highly symmetric peak of the control resin, the bandshape relative to the modified resin displays an evident asymmetry, due to the presence of two components differing in intensity. Clearly, the epoxy groups originating from the DGEBA and those bound to the OG-POSS cages can now be resolved, due to their comparable relative intensity and to the different peak positions. This is confirmed by a curve-fitting analysis of the spectral profiles, whose results are reported in Fig. 9a and b.

It is found that the epoxy band of the modified resin can be successfully fitted with a minimum of two Gaussian components and that the spectral parameters of the component at lower wavenumbers (FWHH, position, bandshape) are very close to those of the single peak sufficient to simulate the profile in the spectrum of the control resin. The time evolution of the epoxy band in the OG-POSS containing formulation (see inset of Fig. 10) evidences that the higher frequency components decreases to a larger extent with respect to that at lower frequency, thus indicating a higher reactivity of the DGEBA epoxy groups with respect to those of the OG-POSS. A quantitative analysis has been performed by curve fitting the sequence of spectra in the inset of Fig. 10. Assuming a close value of molar absorptivity for the two kinds of oxirane rings (assumption justified by the similarity of the molecular structure in the vicinity of the epoxy group) it is possible to convert the absorbance values of the two components into their relative conversions. The results of this analysis are presented in Fig. 10 and quantitatively evidence the different reactivity of the two epoxy species. It is explicitly noted that this analysis can only be performed in the post-curing stage, since in the curing stage the profile of the epoxy band is dominated by the more intense DGEBA component (80%, initially), which prevents resolution. From the data of Fig. 10 it can be deduced that at the end of the cure cycle the epoxy DGEBA conversion (α_{DGEBA}) is 0.98, while the epoxy OG-POSS conversion (α_{POSS}) is 0.93. After post-curing α_{DGEBA} is 0.99 and α_{POSS} is 0.97.

It is likely that in the higher conversion regimes, when the molecular mobility of the system is severely restricted, the more sterically hindered epoxy groups linked to the OG-POSS cages possess a reduced tendency to react with secondary amine and/or O–H groups in comparison to residual DGEBA epoxies present as dangling chains in the cross-linked network.

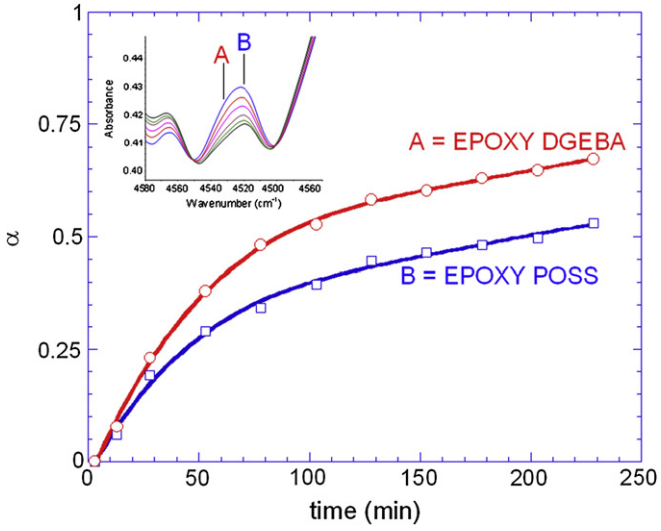

Fig. 10. Relative conversion of the epoxy groups of DGEBA (red curve) and OG-POSS (blue curve) as a function of time for the post-curing at 180 °C. mixture composition DGEBA/DDS/OG-POSS 56/24/20 wt%. (For interpretation of the references to colour in this figure legend, the reader is referred to the web version of this article.)

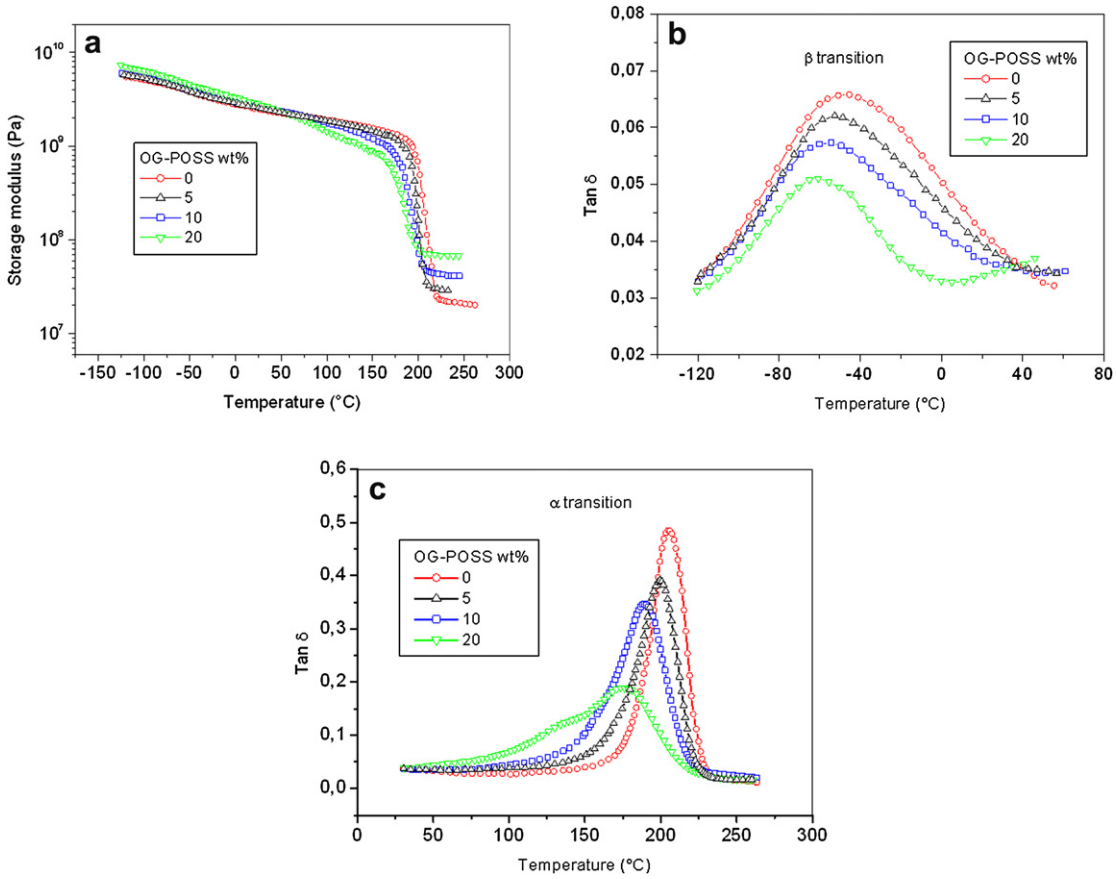

Fig. 11. (a) Storage modulus (E') as a function of temperature for the control resin and the nanocomposites. (b) Loss factor (tan δ) as function of temperature in the range −120 °C to +60 °C for the control epoxy resin and nanocomposites. (c) Loss factor (tan δ) as function of temperature in the range 30 °C–300 °C for the control epoxy resin and nanocomposites.

3.3. Viscoelastic analysis

3.3.1. Dynamic-mechanical properties

The dynamic-mechanical spectra in terms of storage modulus (E') and loss factor (tan δ) at 1 Hz for the control DGEBA/DDS resin and for epoxy nanocomposites containing different amount of OG-POSS are reported in Fig. 11a–c. The tan δ plots (Fig. 11 b and c) show the occurrence of two distinct relaxations with increasing temperature. The relaxation taking places between −100 °C and +50 °C is commonly referred to as the β transition, while the relaxation appearing at higher temperature is an α transition process and corresponds to the glass transition temperature (T_g). In fact, in this region the storage modulus (Fig. 11a) exhibits a sharp drop and then approaches a constant value (rubbery plateau). Fig. 11a also shows that E' is not constant at $T < T_g$ but it slightly decreases with temperature. Most likely the residual stress field due to the different thermal expansion coefficients of epoxy resin

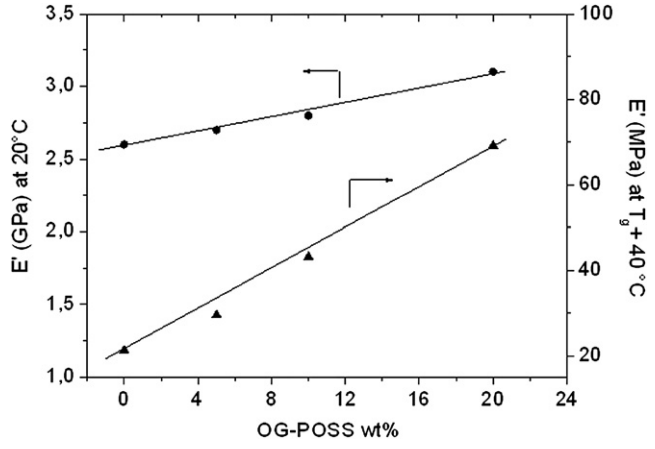

Fig. 12. Storage modulus (E') at 20 °C and at 40 °C above T_g as a function of the OG-POSS content.

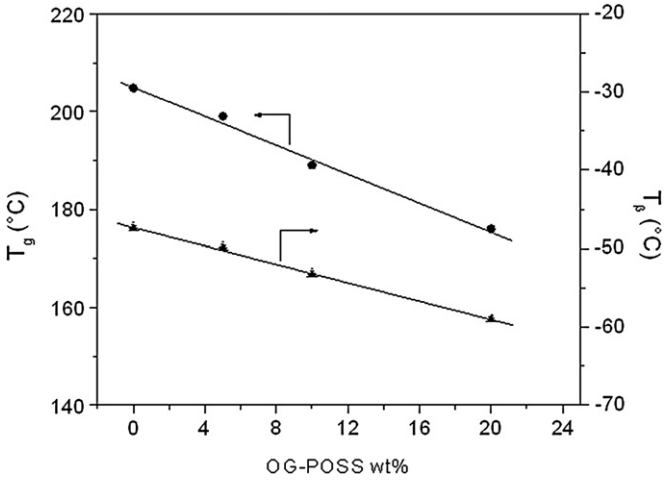

Fig. 13. Glass transition temperature (T_g) and β transition temperature (T_β) determined from the tan δ peak as a function of the OG-POSS content.

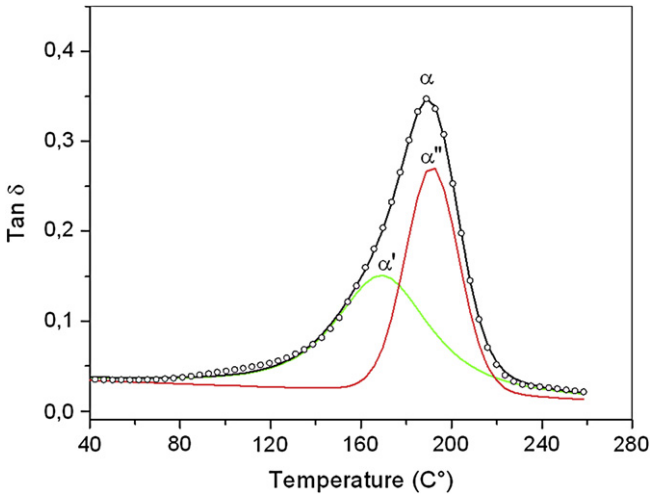

Fig. 14. Curve-fitting analysis of the α transition of the nanocomposite with 10 wt% of OG-POSS. The figure displays the experimental data (○), the fitted profile (solid line), and the resolved peak components (α′ and α″).

and OG-POSS may induce relaxations in the polymeric matrix which account for the negative slope of E' versus temperature. Therefore, the values of E' in the glassy region were measured by extrapolating the low temperature E' linear trend up to the peak temperature of the loss factor curve, assumed as T_g.

The data of Fig. 11 show clearly that the incorporation of OG-POSS in the epoxy network induces noticeable changes in the dynamic-mechanical parameters. First, as demonstrated in Fig. 12, the storage modulus, evaluated at $T = 20\,^{\circ}C$ and at $T_g + 40\,^{\circ}C$ increases with increasing the OG-POSS concentration. This enhancement is higher in the rubbery state than in the glassy region, ensuring a better high temperature performance of the hybrids with respect to the neat epoxy resin. It is known that for epoxy resins the modulus increases with increasing the crosslink density. For epoxy/OG-POSS nanocomposites the crosslink density is expected to decrease owing to the high mass and the large volume of OG-POSS units. Therefore, the increased modulus can be essentially ascribed to a reinforcing effect of the rigid OG-POSS nanocages. This reinforcement is less pronounced at $T < T_g$ because in the glassy state the modulus is mainly dependent on the interaction between chains rather than on the crosslink density.

A second observation arises from Fig. 13, where the values of T_g and T_β, determined from the maxima of the tan δ curves, are presented as a function of OG-POSS content. This plot shows that both T_g and T_β decrease steadily with increasing the OG-POSS concentration. In terms of T_g the addition of 20 wt% of OG-POSS reduces the T_g of about 30 °C, whereas the decrease in T_β is in the order of 11 °C.

The lowering of glass transition was found in several epoxy/OG-POSS systems and in many cases it was attributed to incomplete curing of the epoxy matrix, resulting from the inclusion of OG-POSS [36–38]. In the present case the FT-NIR analysis demonstrated that, after curing and post-curing, the conversion of the epoxy groups for both the control resin and the nanocomposites was almost complete. Therefore, the lowering of T_g must be ascribed to the OG-POSS moieties incorporated in the epoxy network. In particular, two contributions may arise from the OG-POSS addition. One, as mentioned before, is related to the large volume of the OG-POSS nanocages, and the other is due to the flexible organic groups bound to the OG-POSS cage (eight aliphatic propyl-diglycidyl ether groups per OG-POSS molecule) that, acting as soft junctions in the epoxy network permit easier chain segmental movement. The net result is the formation of networks with enhanced chain mobility and decreased crosslink density. Accordingly, lower glass transition temperatures are achieved with respect to the control resin.

A further consideration is given by the tan δ curves depicted in Fig. 11c. Addition of OG-POSS broadens the α transition and decreases its intensity, In particular, for an OG-POSS concentration of 20 wt% a new relaxation, in the range 120 °C–150 °C, appears as a shoulder of the principal peak. This broadening is indicative of an increased heterogeneity of the network structure as the OG-POSS content increases. A curve-fitting analysis of the spectra of Fig. 11c shows that not only the hybrids, but also the control epoxy resin exhibits a shoulder (α′) in the lower temperature side. An example of this analysis is shown in Fig. 14 for a system containing 10 wt% of OG-POSS. In Fig. 15 are presented the main characteristics of the resolved peak components (α′ and α″). It is apparent that, with increasing the OG-POSS content, the FWHH of both α′ and α″ peaks increases (Fig. 15a). Furthermore, the area of the α′ peak increases, while that of the α″ peak decreases. The total area of the two peaks remains essentially constant with OG-POSS loading (Fig. 15b). These findings [38,39] give an insight into the structure evolution of the networks. It has been demonstrated that the formation of epoxy/OG-POSS hybrids from epoxy functionalized OG-POSS is controlled by the competition between the aggregation tendency of OG-POSS monomers and their reactive incorporation within the epoxy network. Generally, aggregation or even crystallization of OG-POSS units occurs when there is a poor compatibility with the organic matrix. In our case, all the investigated hybrids were found homogeneous and visually transparent after the curing and post-

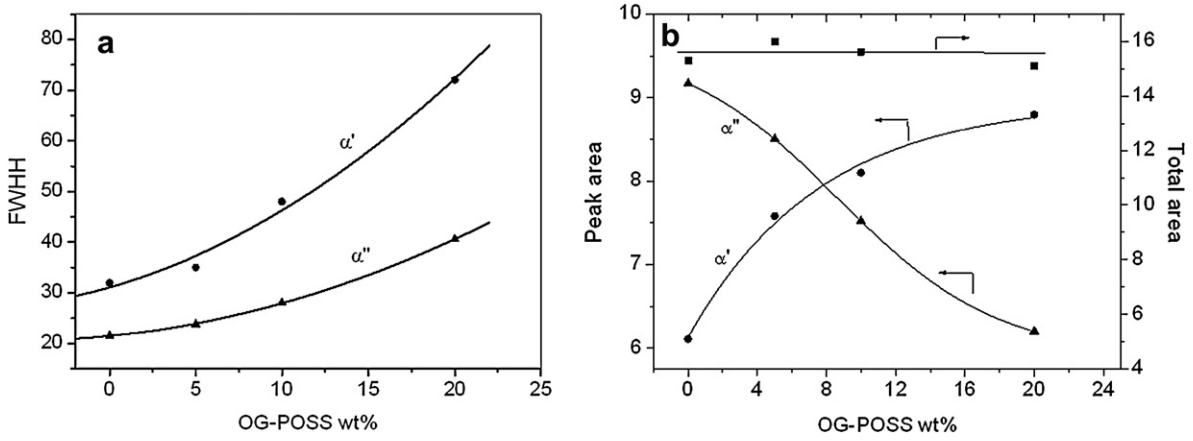

Fig. 15. Characteristics of α′ and α″ peaks as a function of the OG-POSS content. (a) FWHH; (b) peak area and total area.

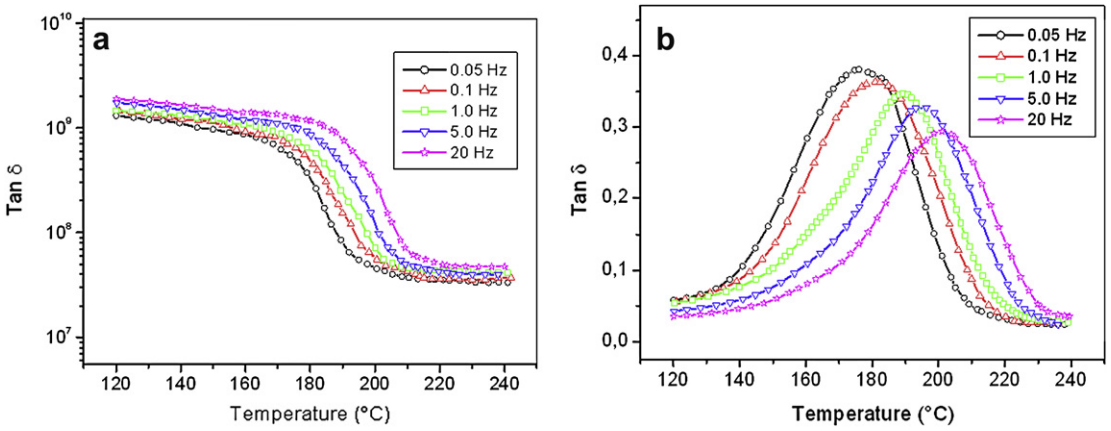

Fig. 16. (a) Storage modulus as a function of temperature in the range 120–240 °C, for the nanocomposite with 10 wt% of OG-POSS. Measurements made at different frequencies, as indicated. (b) Loss factor (tan δ) a function of temperature in the range 120–240 °C, for the nanocomposite with 10 wt% of OG-POSS. Measurements made at different frequencies, as indicated.

curing processes, suggesting a complete miscibility of OG-POSS with the DGEBA/DDS reactive admixture before and after the network formation. On this basis and considering the previously discussed spectroscopic evidences, it can be assumed that the OG-POSS units are readily incorporated into the network structures. The size of these moieties is comparable to those of a random coil but considerably smaller than those of a DGEBA/DDS chain segment between two cross-link points. The net effect of the presence of these defects within the network is to broaden the distribution of relaxation times, manifested in the enlargement of the α-relaxation peak. As the OG-POSS content increases there is a tendency to form a phase richer in OG-POSS which, because of its increasing defectiveness and chain mobility, displays a lower T_g. In fact, the broadening of the α-peaks is not symmetrical but occurs preferentially in the lower temperature side. At a OG-POSS content of 20 wt% the above regions have grown enough to form a distinct network whose α transition can be readily resolved from that of the DGEBA/DDS rich phase. However the above is to be regarded as a nanophase separation process, since, as already mentioned, the system remains visually transparent and, to any respect, homogeneous.

It is to be remarked the superior sensitivity of the dynamic-mechanical analysis in detecting the occurrence of etherophases in the nanometer domain which remain elusive and extremely difficult to identify both with electron microscopy techniques (TEM, ESEM) and with X-ray scattering methods (SAXS).[21,40].

3.3.2. Glass–rubber relaxation process

To further investigate the effect of OG-POSS on the main relaxation and to quantify molecular parameters related to the networks, dynamic-mechanical measurements in the glass–rubber region at different frequency were performed. As an example, in Fig. 16 are shown the dynamic-mechanical spectra in terms of storage modulus and tan δ, collected at different frequencies for a nanocomposite with 10 wt% of OG-POSS. Time–temperature superposition [41,42] was applied in order to obtain master curves versus frequency across the α transition. Fig. 17 illustrates the isotherms, obtained from Fig. 16, as a function of frequency in the temperature range: $T_g - 30$ °C and $T_g + 30$ °C. According to the superposition principle, these curves can be shifted along the frequency axis to produce master curves over an extended frequency range at a reference temperature T_0. In Fig. 18 these master curves are shown. It is explicitly noted that no vertical shift was necessary to get a satisfactory superposition; the reference temperature was taken as the T_g at 1 Hz.

In the glass transition region, the temperature dependence of the shift factor, a_T, follows the well-known Williams–Landel–Ferry (WLF) equation [41,42]:

$$\log a_T = -\frac{C_1^g (T - T_g)}{C_2^g + T - T_g} \tag{9}$$

where C_1^g and C_2^g are the values of the viscoelastic coefficients at T_g.

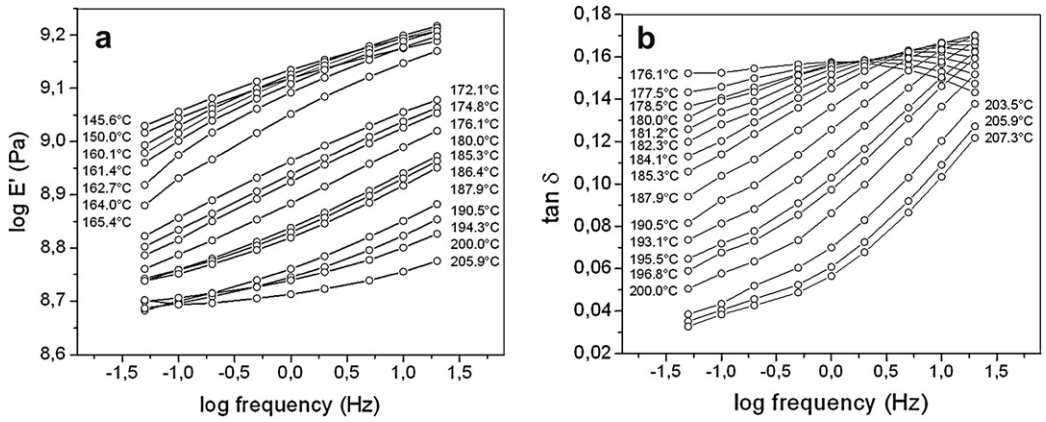

Fig. 17. (a) log E' isotherms as a function of the *log frequency* for the nanocomposite with 10 wt% of OG-POSS. (b) Loss factor (tan δ) isotherms as a function of the *log frequency* for the nanocomposite with 10 wt% of OG-POSS.

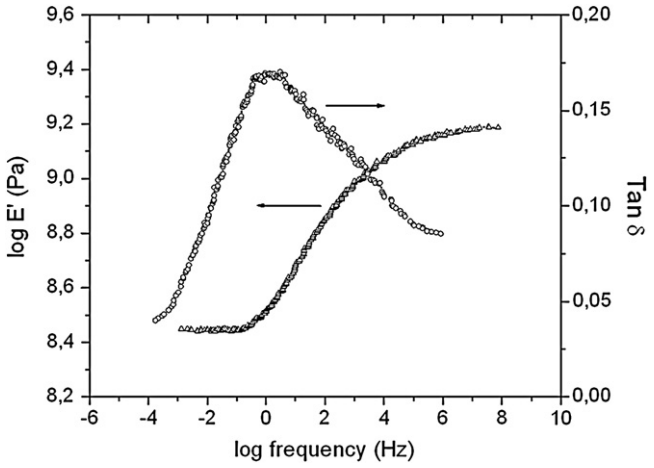

Fig. 18. Master curves for the storage modulus (E') and loss factor ($\tan\delta$) relative to the nanocomposite with 10 wt% of OG-POSS.

According to eq. (9), C_1^g and C_2^g can be determined by plotting $(T-T_g)/\log a_T$ versus $(T-T_g)$ (see Fig. 19). The values of C_1^g and C_2^g relative to the all the investigated networks are summarized in Table 2. The addition of OG-POSS decreases the parameter C_1^g, while the parameter C_2^g is scarcely affected. Although these effects are relatively modest, they provide important information on the structure of the networks, since C_1^g and C_2^g are related to molecular quantities such as the fractional free volume, f_g, available at T_g and the expansion coefficient of the free volume above T_g, α_f:

$$C_1^g = \frac{B}{2.3 f_g} \tag{10}$$

$$C_2^g = \frac{f_g}{\alpha_f} \tag{11}$$

and thus

$$C_1^g \times C_2^g = \frac{B}{2.3\alpha_f} \tag{12}$$

where B is an empirical constant usually taken equal to unity [43,44].

Table 2
Viscoelastic parameters for the control epoxy resin and nanocomposites.

Code	OG-POSS (wt%)	C_1^g (°C)	C_2^g (°C)	$C_1^g \times C_2^g$	$f_g/B \times 10^2$	$\alpha_f/B \times 10^3$
N0	–	13.0	90.5	1170	3.34	0.372
N5	5	12.4	90.1	1116	3.5	0.389
N10	10	11.2	89.7	1005	3.88	0.432
N20	20	9.1	89.1	811	4.77	0.536

As shown in Table 2, both f_g/B and α_f/B increase with increasing the concentration of OG-POSS, indicating that the addition of OG-POSS enhances the free volume and the tendency of the network to undergo thermal expansion. These results confirm our earlier remarks on the effect of OG-POSS in decreasing the T_g. In addition, since f_g is mainly related to the free volume, while α_f depends on chain flexibility, the fact that both parameters increase with OG-POSS content indicates that the relative networks display enhanced free volume and chain flexibility.

The time–temperature characteristics of the networks in the glass transition region were further examined in terms of cooperativity or dynamic fragility [45–47]. Generally, materials that display strong degradation of structure with temperature are designed as "fragile" liquids, and their relaxation typically reflects a high degree of intermolecular interactions. On the contrary, materials with flexible backbones exhibit reduced intermolecular constrains, and, as a result, display less time–temperature sensitivity (lower fragility) [48,49]. The epoxy/OG-POSS hybrids most likely fall between these two categories, since flexible OG-POSS segments are incorporated in a rigid epoxy network.

The fragility parameter, m, is expressed as [48,49]:

$$m = \frac{\mathrm{d}\log a_T}{\mathrm{d}(T_g/T)} \quad \text{at} \quad T = T_g \tag{13}$$

and can be evaluate by the construction of Angell plots [50], normalized Arrhenius plots wherein the shift factor, a_T is reported as $\log a_T$ versus T_g/T in the vicinity of the glass transition. Fig. 20 shows cooperativity plots for the control resin and the nanocomposite networks. The solid curves correspond to WLF fits to the data. The values of m are determined from the first-derivative of the cooperativity curves evaluated at $T = T_g$. The parameter, m, may also be estimated directly from the WLF equation. In fact, combining eqs. (9) and (13) we obtain:

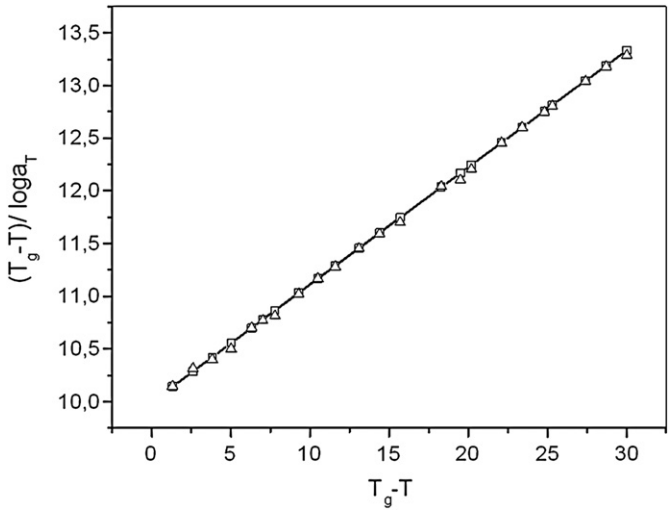

Fig. 19. Evaluation of the viscoelastic parameters C_1^g and C_2^g from the shift factors of the master curves E' (□) and $\tan\delta$ (△) for the nanocomposite with 10 wt% of OG-POSS.

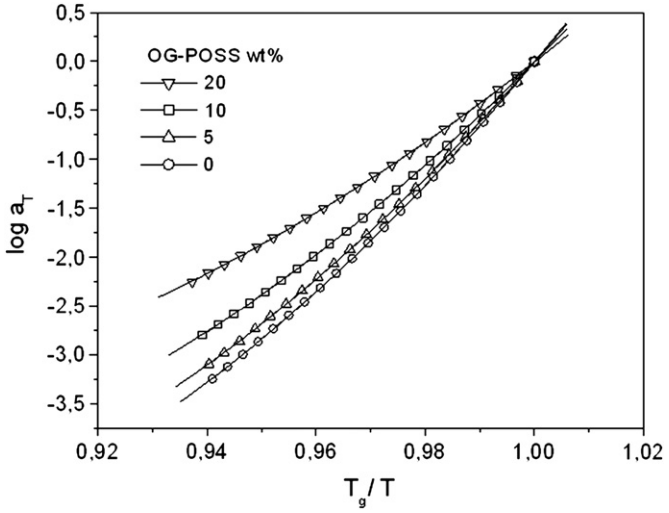

Fig. 20. Cooperativity plots, i.e. $\log a_T$ versus T_g/T, for the pure epoxy resin and nanocomposites with different OG-POSS content, as indicate. Solid curves are WLF fits.

Table 3
Fragility parameter (m) and activation energy ($E_a^{T_g}$) for the control epoxy resin and nanocomposites.

Code	OG-POSS (wt%)	$m = C_1^g T_g / C_2^g$	$m = \frac{d\log a_T}{d(T_g/T)}$	$E_a^{T_g}$ (kJ/mol)
N0	–	68.6	66.4	625.7
N5	5	64.9	62.6	548.8
N10	10	57.7	55.4	508.8
N20	20	45.8	43.1	392.6

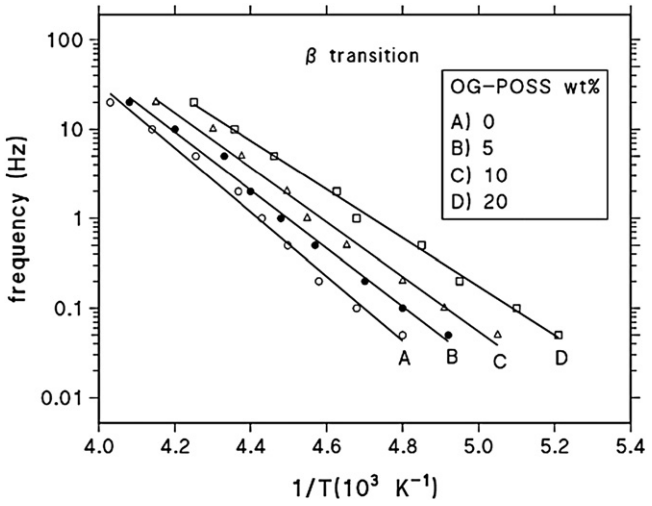

Fig. 21. Arrhenius plots relative to the β transition for the pure epoxy resin and nanocomposites with different OG-POSS content, as indicated.

$$m = \frac{T_g C_1^g}{C_2^g} \tag{14}$$

In Table 3 are reported the values of m determined with both methods, which yield essentially coincident results. A gradual decrease of the fragility index is observed for the hybrid systems with increasing the OG-POSS content. This result indicates a reduction of the intermolecular cooperativity in the glass transition region. The fragility index can also be related to the apparent activation energy, at T_g, $E_a^{T_g}$ [48,49] as:

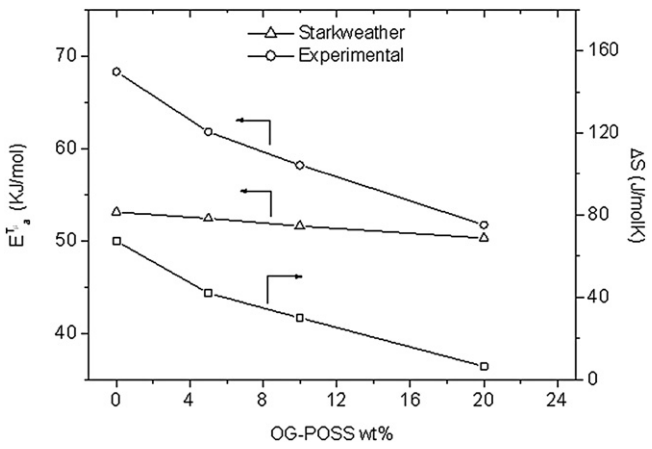

Fig. 22. Activation energy ($E_{a,\beta}$) and activation entropy (ΔS) of the β transition as a function of the OG-POSS content. (○) Experimental data; (△) data from Starkweather method.

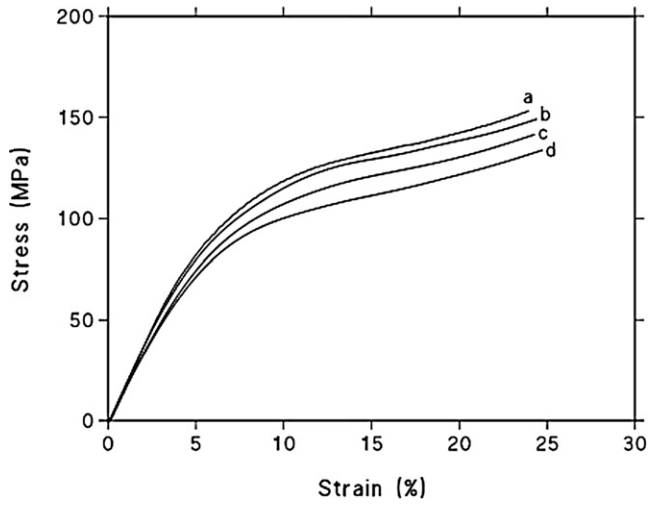

Fig. 23. Compressive stress–strain curves at 20 °C and 1.0 mm/mm. (a) pure epoxy resin; (b) nanocomposite with 5 wt% of OG-POSS; (c) nanocomposite with 10 wt% of OG-POSS; (d) nanocomposite with 20 wt% of OG-POSS.

$$m = \frac{E_a^{T_g}}{2.303RT_g} \tag{15}$$

where R is the universal gas constant.

The values of $E_a^{T_g}$ are listed in Table 3; a significant decrease of activation energy is found for the hybrids in comparison to the neat resin. This result, in accordance to the variation of the fragility index, clearly reflects the role of OG-POSS inclusions in facilitating polymer relaxation processes, through the formation of excess free volume, reduction of the intermolecular interactions and increase in chain flexibility.

3.3.3. β transition

Several literature studies have attributed the β transition in epoxy/diamine networks to the motion of both the hydroxyl-ether structural units (–O–CH_2–CH (OH)–CH_2–) and the phenyl groups of the amine-cured epoxy [51–53]. As reported in Fig. 13, this transition is shifted to lower temperatures with OG-POSS loading. Such a finding, in accordance to the lowering of the T_g, can be attributed to the OG-POSS units that facilitate the localized motions of the structural segments involved in the transition.

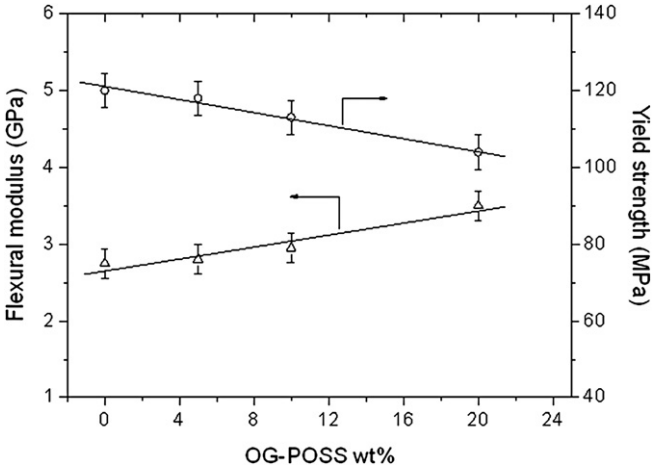

Fig. 24. Flexural modulus and yield strength as a function of the OG-POSS content. Error bars indicate standard deviation over 4 measurements.

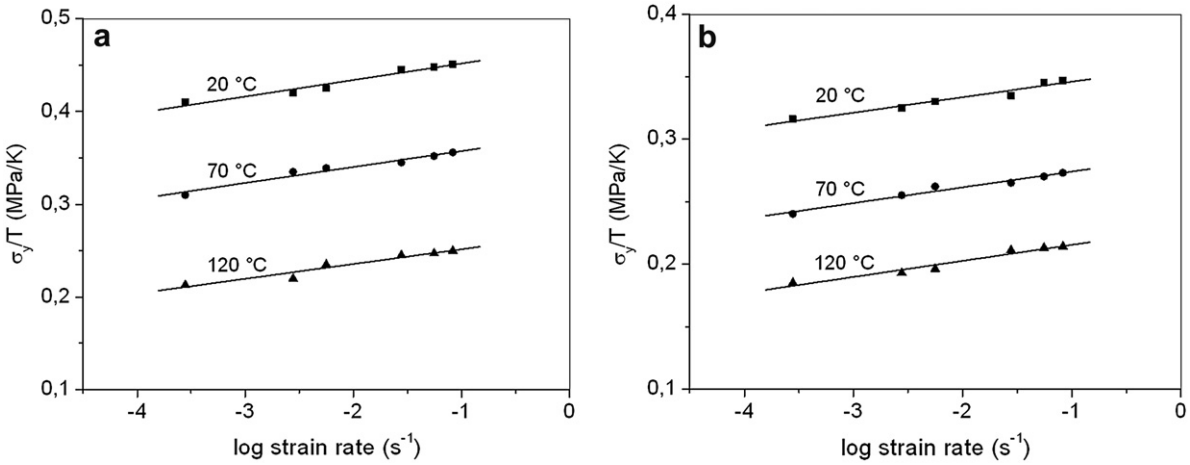

Fig. 25. Eyring plots, i.e. σ_y/T versus log $\dot{\varepsilon}$ for (a) pure epoxy resin; (b) nanocomposite with 10 wt% of OG-POSS.

The activation energy of the transition was evaluated by multi-frequency DMA measurements and by considering an Arrhenius dependence of the type:

$$f = A \times \exp\left(-E_a^{T_\beta}/RT\right) \tag{16}$$

where f is the frequency, A is the pre-exponential factor, T is the relaxation peak temperature and $E_a^{T_\beta}$ is the activation energy.

The $E_a^{T_\beta}$ values determined from the slope of Arrhenius plots (see Fig. 21) are reported in Fig. 22, which points to a decrease of $E_a^{T_\beta}$ with increasing the OG-POSS content.

The linear Arrhenius behaviour of the β relaxation is also indicative of a localized, relatively non-cooperative molecular origin of this transition. Additional insight with respect to its non-cooperative character were obtained considering the approach proposed by Starkweather [54,55], which allows us to separate the activation energy into an activation enthalpy term (ΔH^+) and an activation entropy term (ΔS^+). In particular, Strarkweather found that for many relaxation processes, particularly those involving small segments motions independent of one another, the activation entropy is close to zero. Under this assumption, if the relaxation is at the frequency of 1 Hz and at temperature T', the activation energy, $E_{a,\beta}$, follows a simple, almost linear dependence on temperature [56,57].

$$E_{a,\beta} = RT'\left[1 + \ln(k/2\pi h) + \ln T'\right] \tag{17}$$

where k and h are the Boltzmann and Planck constants, respectively.

The difference between the experimental activation energy and this theoretical value is equal to $T\Delta S^+$. Therefore, eq. (17) defines an effective lower limit for the activation energies of viscoelastic processes below T_g. The data evaluated from eq. (17) are shown in Fig. 22 together with the values of the activation entropy. It is apparent that for the neat resin the activation energy differs significantly from that calculated experimentally, and the value of ΔS^+ is higher than zero. These results indicate that the β transition is not completely localized, but retains a limited cooperative nature. It is noted, however, that, according to Starkweather, ΔS^+ values up to 100 J mol^{-1} K^{-1} are still to be considered characteristic of essentially non-cooperative motions. The addition of OG-POSS progressively decreases the activation entropy making the β transition fully localized for the composite with 20 wt% of OG-POSS. The reduced cooperativity can be ascribed, again, to a reduction of inter- and intramolecular interactions in the network brought about by the OG-POSS units.

3.4. Mechanical and fracture properties

Typical compressive stress–strain curves for the pure epoxy resin and nanocomposites are shown in Fig. 23. The compressive yield strength, evaluated as reported in the experimental section, together with the flexural modulus is reported in Fig. 24 as a function of the OG-POSS concentration. In general, the values of the static flexural modulus are close (slightly higher) to those evaluated by the dynamic technique, which employs a similar geometry. As it was found in the DMA experiments, the modulus increases linearly with increasing OG-POSS content. An opposite trend is observed for the yield strength. As an example, the modulus of the hybrid with 20 wt% of OG-POSS is 27.3% higher than that of the neat resin, whereas its yield strength is about 19% smaller. Therefore, the epoxy network seems to become stiffer and tougher upon OG-POSS loading.

To further investigate the yielding behaviour, the thermodynamic properties for yielding were evaluated. Compressive mechanical tests at different strain rates and temperatures were performed and the results were analyzed by application of the Eyring theory. The basis of this approach is that the yielding is an energy activated process involving the motion of molecular segments under the effect of external stresses. The Eyring model predicts the following relationship between strain rate, $\dot{\varepsilon}$, and yield stress, σ_y, [58,59]:

$$\frac{\sigma_y}{T} = \frac{E^*}{V^*T} + \frac{2.303R}{V^*}\log\frac{\dot{\varepsilon}}{A} \tag{18}$$

where V^* and E^* are the activation volume and the activation energy, respectively, and A is a material's constant.

According to eq. (18), plots of σ_y/T versus log $\dot{\varepsilon}$ give a set of parallel lines for measurements conduced at different temperatures. This is shown in Fig. 25 for the neat epoxy resin and for the

Table 4
The yielding activation energy (E^*) and activation volume (V^*) for the control epoxy resin and nanocomposites.

Code	OG-POSS (wt%)	Activation energy (E^*) kJ/mol	Activation volume (V^*) nm^3
N0	–	308	1.98
N5	5.0	272	2.26
N10	10	237	2.65
N20	20	225	3.2

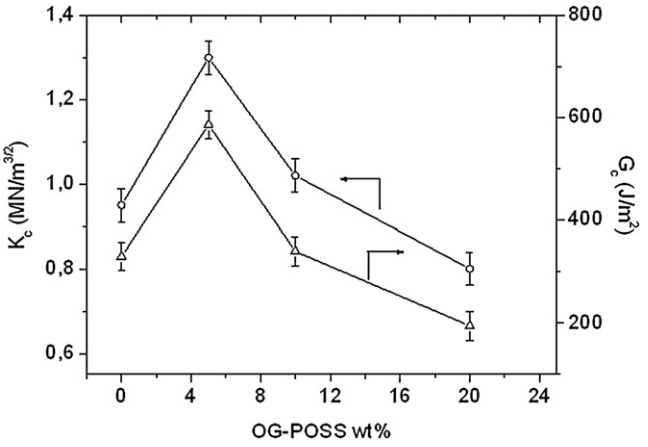

Fig. 26. Variation of the critical stress intensity factor, K_c, and the critical strain energy release rate, G_c, as a function of the OG-POSS content. Error bars indicate standard deviation over 3 measurements.

composite with 10 wt% of OG-POSS. Similar plots were found for nanocomposites with 5 and 20 wt% of OG-POSS. From the slope and intercept of the Eyring plots, V^* and E^* were determined and their values are reported in Table 4. The correlation coefficients for the calculated values over the range of strain rates and temperatures investigated are higher than 0.98 in all cases. The data of Table 4 show that the activation volume increases and the activation energy decreases with increasing OG-POSS content. This behaviour can be explained from considerations of the length scale of the segmental motions of the epoxy network involved in the yielding process. In particular, the enhancement in the activation volume implies that a larger number of chains segments are interested in the yield process as the OG-POSS content increases. This is the result of an increased chain mobility of the segments involved in the yielding process, due to the flexible OG-POSS groups incorporated into the epoxy network. At the same time the enhanced network mobility causes the energy barrier for yielding to decrease, resulting in lower activation energy values. Thus, the effect of OG-POSS on the yielding behaviour is analogous to that outlined earlier for the relaxation processes in dynamic-mechanical tests.

Since the yield stress of the nanocomposites decreases with OG-POSS loading, a corresponding increase in fracture toughness is to be expected. In Fig. 26 are reported the values of the critical stress intensity factor, K_c, and of the critical strain energy release rate, G_c, as a function of OG-POSS content. This plot shows that both K_c and G_c increase significantly up to an OG-POSS content of 5 wt%, while at higher loadings a marked reduction in these parameters is observed. In terms of G_c the addition of 5 wt% of OG-POSS enhances the fracture toughness of the epoxy matrix by 200%, while for a OG-POSS content of 20 wt% the toughness decrease by about 50%. To further investigate the fracture behaviour, the surfaces of fractured samples were examined by Scanning Electronic Microscopy (SEM). In Fig. 27 are compared the SEM micrographs, taken near the crack tip, of the control resin and of nanocomposites with 5 and 20 wt% of OG-POSS. The unmodified epoxy resin (Fig. 27a) exhibits a relatively smooth fracture surface with the presence of only large striations in the direction of crack growth (crack propagates from left to right of micrographs). These fracture patterns, typical of brittle thermosets, are mainly generated via a shear yielding mechanism, which represents the major source of energy dissipation in epoxy resin systems [60,61]. The contribution of this mechanism to energy dissipation is found to be strongly dependent on OG-POSS concentration. In fact, at 5 wt% of OG-POSS (Fig. 27b)

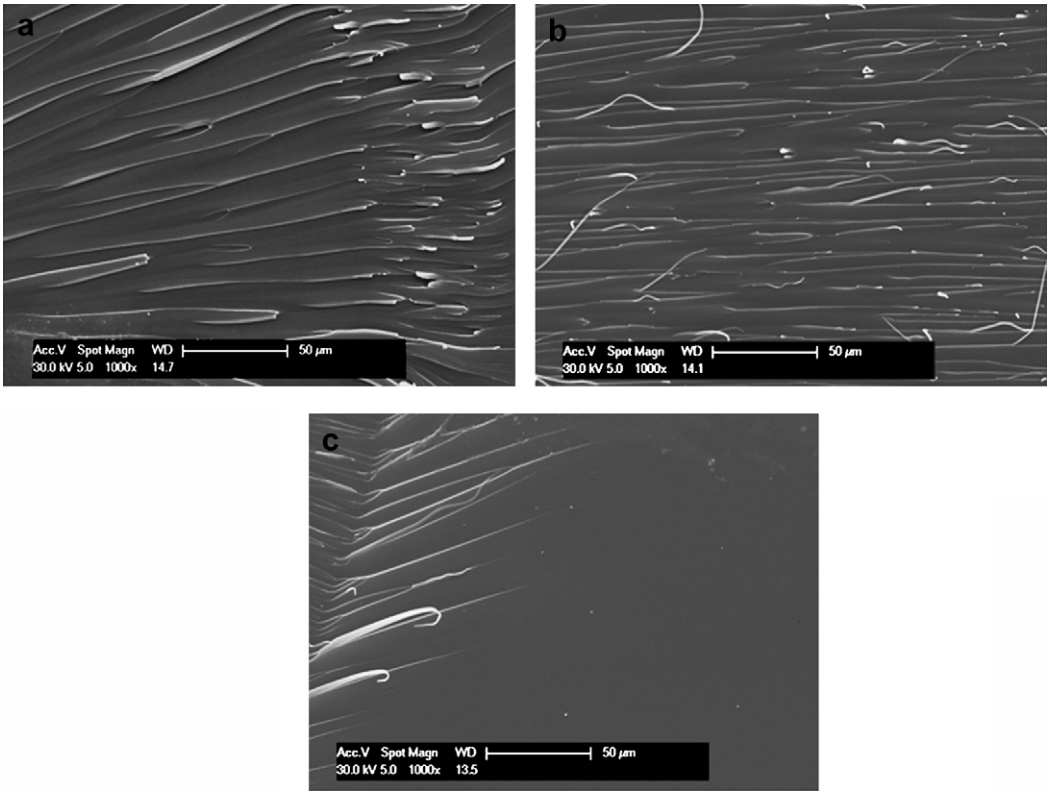

Fig. 27. SEM pictures of fractured surfaces: (a) pure epoxy resin; (b) nanocomposite with 5 wt% of OG-POSS; (c) nanocomposite with 20 wt% of OG-POSS.

the fracture surface appears completely covered by closely spaced striations, indicating an extensive plastic shear flow of the matrix. On the other hand, at 20 wt% of OG-POSS (Fig. 27c) the fracture surface is very smooth and featureless with no apparent signs of localized plastic deformations, apart from few striations confined in a small area ahead of the crack tip. According to the viscoelastic analysis, the toughening enhancement at low OG-POSS content can be mainly attributed to the flexible OG-POSS segments incorporated into the epoxy network, which enhance its ability to be plastically deformed prior to fracture. At increasing OG-POSS contents this effect is counteracted by the formation of OG-POSS reach regions, which provide low energy paths for crack propagation. In addition, the OG-POSS nanocages, acting as weak points, may facilitate the formation and growth of cracks. All these effects lead to a premature fracture of the nanocomposite, which accounts for the lowering in toughness.

4. Conclusions

In the present investigation a thermosetting system consisting of DGBA/DDS and various amounts of epoxidized OG-POSS was prepared and characterized in terms of reactivity, viscoelastic behaviour and mechanical properties. The following conclusions were drawn:

- FT-NIR spectroscopy demonstrated that the epoxy groups of OG-POSS were almost as reactive as those of the DGEBA towards the amine functionalities in the curing stage, thus ensuring the incorporation of the OG-POSS cages within the organic network. However, in the post-curing step, a lower reactivity of the OG-POSS epoxies was found, possibly due to steric hindrance effects.
- The dynamic-mechanical analysis showed an increase in the storage modulus in both glassy and rubbery regions, which was attributed to a reinforcing effect of the OG-POSS nanocages. On the other hand, T_g and T_β decreased with OG-POSS content.
- The viscoelastic analysis in the T_g region by multi-frequency measurements allowed us to determine free volume related parameters and to deepen the interpretation of the network's molecular architecture. It was found that the addition of OG-POSS enhanced the free volume and the tendency of the network to undergo thermal expansion. At the same time, the cooperativity or dynamic fragility was found to decrease with increasing the OG-POSS content. The sub-T_g transition (β) was also affected by the OG-POSS addition: a reduction of activation entropy was found by increasing the OG-POSS content, which made the transition fully localized. This effect was attributed to a reduction of inter- and intramolecular interactions in the network brought about by the OG-POSS units.
- The yield behaviour evidenced an increase of the activation volume and a corresponding decrease of the activation energy with increasing the OG-POSS content, which was attributed to an enhancement of the chain mobility of the segments involved in the yielding process. Fracture measurements showed an improvement of the relevant parameters (K_c and G_c) up to a critical concentration of OG-POSS (5 wt%), after which a decrease of toughness was observed. These results were in agreement with the fractographic analysis.

References

[1] Mascia L. The role of additives in plastics. London: Edward Arnold; 1974. p. 87–8.
[2] Rothon R. Particulate fillers for polymers. Shrewsbury: RAPRA Technology; 2002.
[3] Davidson T. Conductive and magnetic fillers. In: Xanthos M, editor. Functional fillers for plastics. Weinheim, Germany: Wiley-VCH; 2005.
[4] Brown EN, White SR, Sottos NRJ. Mat Sci 2004;39:1703.
[5] Azimi HR, Pearson RA, Hertzberg RW. Polym Eng Sci 1996;36:2352.
[6] Wang MS, Pinnavaia TJ. Chem Mater 2004;6:468.
[7] Giannelis EP. Adv Mater 1996;8:29.
[8] Wu J, Mather PT. J Mokromol Sci C, Polym Rev 2009;49:25.
[9] Strachota A, Whelan P, Kriz J, Brus J, Urbanova M, Slouf M, et al. Polymer 2007;48:3041.
[10] Bian Y, Mijovich J. Macromolecules 2008;41:7122.
[11] Choi J, Harcup J, Yee AF, Zhu Q, Laine RM. J Am Chem Soc 2001;123:11420.
[12] Ni Y, Zheng S. Polymer 2004;45:5557.
[13] Choi J, Yee AF, Laine RM. Macromolecules 2004;37:3267.
[14] Liu Y, Zheng S, Nie K. Polymer 2005;46:12016.
[15] Haddad TS, Lee A, Philips SH. Polym Prep (ACS Div Polym Chem) 2001;42:88.
[16] Lee A, Lichtenhan JD. Macromolecules 1998;31:4970.
[17] Haddad TS, Lichtenhan JD. Macromolecules 1996;29:7302.
[18] Choi J, Kim SG, Laine RM. Macromolecules 2004;37:99.
[19] Choi J, Yee AF, Laine RM. Macromolecules 2003;36:5666.
[20] Choi J, Tamaki R, Kim SG, Laine RM. Chem Mater 2003;15:3365.
[21] Matejka L, Strachota A, Plestil J, Wheland P, Steinhart M, Slaof M. Macromolecules 2004;37:9449.
[22] Strachota A, Kroutilova I, Kovarova J, Matejka L. Macromolecules 2004;38:9457.
[23] Liu H, Zheng S, Nie K. Macromolecules 2005;38:5088.
[24] Brow F, Srawley J. ASTM Spec Tech Publ 1966;510:13.
[25] Plati E, Williams JG. Polym Eng Sci 1975;15:470.
[26] Billaud C, Vandeuren M, Legras R, Carlier V. Appl Spectrosc 2002;56:1413.
[27] Li L, Wu Q, Li S, Wu P. Appl Spectrosc 2008;62:1129.
[28] Siesler HW, Ozaki Y, Kawata H, Heise HM. Near-infrared spectroscopy. Weinheim, Germany: Wiley-VCH; 2004.
[29] Min BG, Stachurski ZH, Hodgkin JH, Heat GR. Polymer 1993;34:3620.
[30] Horie K, Hiura H, Sawada M, Mita I, Kambe HJ. Polym Sci Part A1: Polym Chem 1970;8:1357.
[31] Kamal MR. Polym Eng Sci 1973;13:59.
[32] Kamal MR. Polym Eng Sci 1974;14:231.
[33] Cole KC. Macromolecules 1991;24:3093.
[34] Musto P, Martuscelli E, Ragosta G, Russo P, Villano P. J Appl Polym Sci 1999;74:532.
[35] Musto P, Martuscelli E, Ragosta G, Mascia L. Polymer 2001;42:5189.
[36] Bajaj P, Jhan NH, Ananda Kumar R. J Appl Polym Sci 1990;40:203.
[37] Li GZ, Wang L, Toghiani H, Daulton TL, Koyama K, Pittman Jr CU. Macromolecules 2001;34:8686.
[38] Abad MJ, Barral L, Fasce DF, Williams RJJ. Macromolecules 2003;36:3128.
[39] Patrick TM, Hong GJ, Romo-Uribe A. Macromolecules 1999;32:1194.
[40] Strachota A, Whelan P, Kriz J, Brus J, Urbanova M. Polymer 2007;48:3041.
[41] Williams ML, Landell RF, Ferry JDJ. Am Chem Soc 1955;77:3701.
[42] Ferry JD. Viscoelastic properties of polymers. New York: J. Wiley; 1980.
[43] Heux L, Halary JL, Laupretre F, Monnerie L. Polymer 1997;38:1767.
[44] Gerard JF, Galy J, Pascault JP, Cukierman S, Halary JL. Polym Eng Sci 1991;31:615.
[45] Mijovic J. J Non-Crystalline Solids 1998;235:587.
[46] Couderc H, Delbreilh L, Saiter A, Grenet J, De Souza N, Saiter JMJ. J Non-Crystalline Solids 2007;353:4334.
[47] Qazvini NT, Mohammadi N. Polymer 2005;46:9096.
[48] Kalakkunnath S, Kalika DS, Lin H, Freeman BD. Macromolecules 2005;38:9679.
[49] Xian G, Karbhari VM. Polym Degrad Stab 2007;92:1650.
[50] Angell CA. In: Ngai KI, Wright GB, editors. Relaxation in complex systems. Washington, DC: Naval Research Laboratory; 1984.
[51] Keenan JD, Seferis JC. J Appl Polym Sci 1979;24:2375.
[52] Cukierman S, Halary JL, Monnerie L. Polym Eng Sci 1991;31:1476.
[53] Becker O, Varley R, Simon G. Polymer 2002;43:4365.
[54] Starkweather HWJ. Polymer 1991;32:2443.
[55] Starkweather HWJ. Macromolecules 1990;23:328.
[56] Qu W, Kao TM, Vora RH, Chung TS. Polymer 2001;42:6393.
[57] Schroeder JA, Madsen PA, Foister RT. Polymer 1987;28:929.
[58] MacCrum NG, Buckley CP, Bucknall CB. Principles of polymer engineering. New York: Oxford Science Publishers; 1977.
[59] Ward IMJ. Mat Sci 1971;6:1397.
[60] Kinloch AJ, Shaw SJ, Hunston D. Polymer 1983;24:1355.
[61] Ragosta G, Abbate M, Musto P, Scarinzi G, Mascia L. Polymer 2005;46:10506.